Research Square

Preprints are preliminary reports that have not undergone peer review.
They should not be considered conclusive, used to inform clinical practice,
or referenced by the media as validated information.

Evaluation of WRF Microphysics Schemes for Simulating Lightning and Rainfall over the Complex Terrain of the Western Himalayan Region

Sanjeev Kumar
Indian Institute of Tropical Meteorology
N. Umakanth
Indian Institute of Tropical Meteorology
Alok Sagar Gautam
Hemwati Nandan Bahuguna Garhwal University
Swapnil S. Potdar
Indian Institute of Tropical Meteorology
Rupraj Biswasharma
ruprajaus@gmail.com

Indian Institute of Tropical Meteorology
Karan Singh
Indian Institute of Tropical Meteorology
Devendraa Siingh
Indian Institute of Tropical Meteorology
R P Singh
Banaras Hindu University

Research Article

Keywords: Lightning simulation, Cloud microphysics, WRF model, Western Himalaya, Mixed-phase processes, Extreme convection

Posted Date: May 14th, 2026

DOI: https://doi.org/10.21203/rs.3.rs-9085936/v1

License: This work is licensed under a Creative Commons Attribution 4.0 International License.
Read Full License

Additional Declarations: No competing interests reported.

Abstract

Lightning causes substantial loss of life and infrastructure damage each year. This study presents the first numerical simulation of a severe pre-monsoon thunderstorm that occurred on 23 May 2023 over the complex western Himalayan region (WHR). We evaluate the performance of four WRF microphysics (MP) schemes in simulating lightning and rainfall using ground-based lightning observations and satellite-observed rainfall data. All MP schemes capture the observed temporal variability of lightning, but with notable differences in magnitude, timing, and variability. The Morrison scheme reproduces the timing of peak lightning activity at 15:00 UTC but substantially overestimates flash rates, whereas the Thompson, WDM5, and WSM6 schemes simulate the peak 1–2 hours earlier. Spatial analysis reveals dominant lightning activity along the Himalayan foothills, which is reasonably represented by all MP schemes. Morrisonve phase, Morrison and Thompson simulate enhanced cloud water mixing ratios, supporting latent heat release and sustained convection. Elevated mixing ratios of rainwater, snow, and ice further indicate active mixed-phase processes favorable for cloud electrification. Temporal and spatial evaluations show that Thompson provides the closest agreement with observed lightning variability, while Morrison exhibits higher variability and false detections. Rainfall evaluation indicates improved detection skill for WSM6 and Morrison. Overall, the results demonstrate that no single microphysics scheme consistently outperforms others for both lightning and rainfall, highlighting non-uniform model skill across processes. These findings emphasize the need for region-specific and process-oriented tuning of model physics to improve lightning and rainfall simulations over complex mountainous terrain.

1 Introduction

Lightning events are a common atmospheric phenomenon that poses a major natural hazard during the pre-monsoon season in India (Halder et al. 2015; Siingh et al. 2015; Kumar et al. 2017; Kamra and Kumar, 2020). Each year, lightning strikes result in significant loss of human life and damage to infrastructure. Globally, lightning is responsible for an estimated 6000 to 24000 fatalities annually (Cooper and Holle, 2018). In India, Mishra et al. (2024) analyzed lightning-related fatalities using National Crime Records Bureau data and reported nearly 100000 deaths between 1967 and 2020, with an average of ~ 1876 fatalities per year. Lightning predominantly originates within cumulonimbus clouds and is govern by thermodynamic, dynamical, and microphysical processes, including land-surface thermal contrasts, frontal lifting, orographic forcing, cloud microphysics, and land-use & land-cover variability (Williams, 1992; Kamra and Kumar, 2020; Kumar et al. 2024; Potdar et al. 2025; Potdar et al. 2026). Numerous laboratory and field experiments have demonstrated that microphysical interactions between graupel and ice crystals play a critical role in charge separation and lightning initiation within the mixed-phase regions of thunderstorms (Takahashi, 1978; Berdeklis and List, 2001; Adamo et al. 2007; Oulkar et al. 2019; Zhao et al. 2024; Biswasharma et al. 2025b). The coexistence of ice particles, graupel, and supercooled liquid water leads to intense collisions that facilitate charge separation and cloud electrification via non-inductive charging Mechanism (Williams et al. 2002; Saunders, 2008; Lund et al. 2009; Siingh et al. 2008, 2011, 2012, 2023; Ghoshal Chowdhury et al. 2025). Therefore, realistic

representation of cloud microphysics (MP) is fundamental for accurate simulation of lightning in numerical weather prediction models. The Weather Research and Forecasting (WRF) model has been widely employed for lightning simulation owing to its ability to resolve mesoscale convective processes (Price and Rind, 1992; Yair et al. 2010; Zepka et al. 2014). The Price-Rind (PR92) lightning parameterization relates lightning flash rates to storm height, while subsequent developments incorporate hydrometeor-based inputs to distinguish intra-cloud and cloud-to-ground lightning (Boccippio et al. 2002; Wong et al. 2013; Giannaros et al. 2015; Dafis et al. 2018; Wang et al. 2018; Choudhury et al. 2020; Mohan et al. 2021; Vani et al. 2022; Kumar et al. 2022). Several studies have demonstrated reasonable skill of the WRF model in simulating lightning and rainfall over India (Halder and Mukhopadhyay, 2016; Choudhury et al. 2020; Mohan et al. 2021; Kumar et al. 2023). However, statistical evaluation metrics such as Probability of Detection (POD), False Alarm Ratio (FAR), Bias Score (BIAS), and Critical Success Index (CSI) consistently indicate strong sensitivity to selection of MP scheme, cumulus parameterization, and model resolution (Hazra et al. 2013; Kumar et al. 2023). Different MP schemes represent mixed-phase processes, ice growth, and hydrometeor interactions in fundamentally different ways, directly influencing charge separation, lightning production, and precipitation efficiency. For example, the Morrison scheme incorporates a more detailed treatment of ice-phase and riming processes, whereas WSM6 employs a simpler bulk representation, leading to systematic differences in simulated electrification and rainfall outcomes (Morrison et al. 2009; Hong and Lim, 2006). As a result, schemes optimized for lightning generation do not necessarily yield superior rainfall simulations, and vice versa. The WHR, encompassing Uttarakhand, Himachal Pradesh, Jammu and Kashmir, and Ladakh, is among the most meteorologically vulnerable regions of India. Complex topography and active synoptic systems make the region highly prone to extreme weather events, including heavy rainfall, cloudbursts, hailstorms, and intense lightning, often resulting in landslides and societal impacts (Penki and Kamra, 2013; Dimri et al. 2017; Kashyap and Behera, 2023; Kumar et al. 2024; Lohan et al. 2025). Lightning activity exhibits pronounced variability during the pre-monsoon and retreating monsoon phases, whereas extreme precipitation is more frequent during the summer monsoon and western-disturbance-dominated periods (Bookhagen et al. 2005; Dimri et al. 2017; Kumar et al. 2024). The interaction of western disturbances, cyclonic circulations, and strong orographic forcing provides favorable conditions for deep convection concurrent lightning and rainfall events (Agnihotri and Singh, 1982; Gangane et al. 2025; Hunt et al. 2025).

Despite the high societal exposure and recurring impacts, comprehensive modeling studies examining lightning characteristics over the complex terrain of the WHR remain scarce. Over complex mountainous terrain, sharp gradients in elevation, moisture convergence, and vertical motion introduce additional uncertainty in the representation of cloud microphysics and storm electrification, making lightning simulation particularly sensitive to model physics and resolution. Moreover, although many studies have evaluated lightning and rainfall separately, the combined and comparative performance of WRF microphysics schemes in simulating both processes has not been systematically investigated. In this study, we present the first modeling-based analysis of a severe lightning event over Uttarakhand and surrounding areas on 23 May 2023, characterized by high lightning activity observed by both ISS-LIS and

the Indian Lightning Location Network (ILLN), and associated human fatalities. Insights from this study are relevant for understanding microphysics-lightning-rainfall interactions in other mountainous and orographically complex regions. The objective of this study is to diagnose the sensitivity of lightning and rainfall simulations to four WRF microphysics schemes (WSM6, Thompson, Morrison, and WDM5) over a complex mountainous environment. Specifically, we address the following research questions:

(1) How well do different microphysics schemes in WRF simulate the temporal and spatial characteristics and storm dynamics of a severe lightning event over the western Himalaya?

(2) Do the same microphysics schemes perform similarly for both lightning and rainfall simulations?

2 Materials and Methods

2.1 Study region

The WHR, encompassing Uttarakhand, Himachal Pradesh, Ladakh, and Jammu and Kashmir, is among the most meteorologically vulnerable regions in India. Its complex terrain, characterized by sharp elevation gradients and deep valleys, together with frequent synoptic-scale disturbances, makes the region highly prone to extreme weather events, including heavy rainfall, cloudbursts, hailstorms, and severe lightning, which frequently trigger landslides and societal impacts (Penki and Kamra, 2013; Dimri et al. 2017; Kashyap and Behera, 2023; Kumar et al. 2024; Lohan et al. 2025). Lightning activity over the WHR exhibits pronounced variability, with enhanced occurrence during the pre-monsoon and retreating monsoon phases, while extreme precipitation is more common during the summer monsoon and western disturbance (WD) dominated periods (Bookhagen et al. 2005; Dimri et al. 2017; Kumar et al. 2024). The interaction of WDs, cyclonic circulations, and strong orographic forcing creates favorable conditions for deep convection, leading to concurrent episodes of severe lightning and intense rainfall (Agnihotri and Singh, 1982; Gangane et al. 2025; Hunt et al. 2025). Given the frequent co-occurrence of multiple high-impact hazards and the associated societal vulnerability, we employ a combination of observational datasets and numerical modeling to examine the characteristics of a severe convective event over WHR in detail.

2.2 Model configuration and evaluation

To perform lightning simulations over WHR, we have used the Advanced Research version of the Weather Research and Forecasting (WRF-ARW) model, version 4.5. WRF model has been developed by the National Centre for Atmospheric Research (NCAR). It is built on the Arakawa-C grid and have terrain-following hydrostatic pressure coordinate system with Coriolis and curvature terms. Model integration has performed using a third-order Runge-Kutta time integration scheme (Skamarock et al. 2008). For this study, a three-domain nested configuration was used as D1: 27 km resolution, D2: 9 km resolution and D3: 3 km resolution (Fig. 1). The ILLN observation shows some limitation of detection efficiency over the upper portion of the D3 domain (Biswasharma et al. 2025b). Thus for the analysis, we have focused on a smaller target domain (TD dashed inner box in Fig. 1). Lightning, associated hydrometeors and rainfall

were simulated using four cloud microphysics (MP) schemes: WRF Single-Moment 6-class (WSM6), Thompson, Morrison two-moment, and WRF Double-Moment 5-class (WDM5), together with the Kain-Fritsch cumulus parameterization scheme. A detailed summary of the WRF model configuration is provided in Table 1.

Table 1
Description of WRF-ARW model configuration

Parameters	**Description**	**References**
Domains Size	27km, 9km, 3km	
No. of vertical levels	40	
Cloud Microphysics (MP) Options	**Scheme**	**Reference**
1) mp_physics option = 8		Thompson et al. (2008)
2) mp_physics option = 10	Thompson	Morrison et al. (2009)
3) mp_physics option =14	Morrison 2-mom WRF	Lim and Hong, (2010)
4) mp_physics option = 6	Double-moment 5-class (WDM5)	Hong and Lim, (2006)
	WRF Single-moment 6-class (WSM6)	
Cumulus Options	**Scheme**	**Reference**
Cumulus physics	Kain-Fritsch	Kain, (2004)
cu_physics = 1		
Land Surface, boundary layer and radiation model Options	**Scheme**	**Reference**
Boundary layer scheme	Yonsei University Scheme	Hong et al. (2006)
bl_pbl_physics = 1		Choudhury et al. (2020)
Land surface model	Noah LSM	Niu et al. (2011)
sf_surface_physics = 2		Yang et al. (2011)
sf_sfclay_physics = 1		
Radiation	Rapid Radiative transfer model	Iacono et al. (2008)
ra_la_physics = 4		
ra_sw_physics = 4		
Time Steps	15 Sec	Choudhury et al. (2020)
Lightning Options	**Scheme**	**Reference**
Lightning_option = 1	Price and Rind	Price and Rind (1992) Choudhury et al. (2020)
Initial boundary condition	NCEP FNL data (1° × 1° spatial resolution)	Vani et al. (2022)

The PR92 is one of the widely used parametrization schemes used for the prediction of flash rate (FR) based on the storm height and specially designed for the ocean and land configurations (Price and Rind 1992). The PR92 formulation expresses flash rate as:

$$\varvec{F}_{\varvec{rc}} = 3.44 \times 10^{-5} \varvec{H}_{\varvec{s}}^{4.9}$$

1

Where, $\varvec{F}_{\varvec{rc}}$: FR (Flash min^{-1}), and H_s : Strom Height

Also, PR92 scheme can be upgraded to calculate the Flash rate by using maximum vertical velocity

$$\varvec{W}_{\varvec{max}} = 1.49 \times \varvec{H}_{\varvec{s}}^{1.09}$$

2

and the corresponding flash rate is calculated as

$$\varvec{F}_{\varvec{rc}} = 5 \times 10^{-6} \varvec{W}_{\varvec{max}}^{4.54}$$

3

The performance of the WRF model have evaluated using contingency table based skill scores (Table S1), including (i) Probability of Detection (POD), (ii) False Alarm Ratio (FAR), (iii) Bias Score (BIAS), (iv) Critical Success Index (CSI), and (v) Accuracy (Wilks, 2011; Vani et al. 2022). Additional details on fractional skill score (FSS) metrics are provided in Kumar et al. (2022) and references therein (Table S2).

2.3 Data

We used ground-based lightning data from the ILLN to assess the model performance. The details regarding the principle and working of IILN are given in Biswasharma et al. 2025b and reference therein. The network operates within a frequency band of 1 Hz to 12 MHz, where the lower frequencies are used to detect CG lightning, and higher frequencies are used to detect IC lightning (Vani et al. 2022). The ILLN has an estimated detection efficiency of 90% for CG lightning flashes and 50% for IC flashes (Biswasharma et al. 2025b). In India, the WRF model has been used over the NE, western ghats (WG) and Indo-Gangetic plains to simulate lightning events and the performance of the model has been evaluated by using ILLN data (Choudhury et al. 2020; Mohan et al. 2021; Kumar et al. 2022; Vani et al. 2022). For the Initial and boundary conditions (IC/BC), we have used Final (FNL) Operational Global Analysis Data, as well as geographic data (elevation, LULC, etc) for the model, which were obtained from the National Centers for Environmental Prediction (NCEP). The rainfall data is obtained from Global Precipitation Measurement (GPM).

3 Result and Discussion

3.1 Event description

Figure S1 represents the monthly lightning flash counts along with daily flash counts in May 2023 observed by ISS-LIS over TD. Relatively higher lightning flash counts (1607) were observed in May month particularly on 23 May 2023. Observation shows 769 flashes in the span of 24 hours. Due to temporal limitations of ISS-LIS, we have further carried out the analysis based on ILLN data. To understand the synaptic condition, we analyzed using geopotential height (m) and wind vectors (m s^{-1}) at 500 hPa on over India and adjacent areas as shown in Fig. 2. A well-marked active WD over northwest (NW) India with a mid-tropospheric trough extending from Iran and Pakistan into northwestern India. The southward dip in geopotential height and cyclonic curvature of westerlies over NE India indicate strong dynamical forcing and upper-level divergence associated with the disturbance. Concurrently, a cyclonic circulation at lower levels cantered over Arabian sea with moist southwesterly flow provided a continuous moisture supply into the WHR. Which promoted increased instability and vertical uplift over WHR, leading to the development of deep convective clouds. The Indian Meteorological Department (IMD) bulletin for the same day also reported thunderstorms, hailstorms, gusty winds (50–60 km h^{-1}), and heavy rainfall over the region between 23 and 25 May (Daily IMD bulletin 23 May 2023). The combination of mid-tropospheric trough, low-level moisture advection, orographic lifting possibly created an ideal environment for the observed severe lightning and rainfall over WHR on 23 May 2023.

3.2 Temporal variations

Figure 3 compares the ground-based ILLN observations with WRF model-simulated lightning flash rates (FR). The case study spans a 36-hours window, covering six hours before and six hours after the event day. This period is divided into three phases as initial (22-May-2023 18:00 UTC to 23-May-2023 07:00 UTC), active (23-May-2023 08:00 UTC to 23-May-2023 20:00 UTC), and decay phase (23-May-2023 21:00 UTC to 24-May-2023 06:00 UTC). During the initial phase, FR was low in both observations and simulations. All MP schemes generally followed the observed variation, although Morrison exhibited some overestimation. In the active phase, lightning activity increased sharply before reaching the peak and then gradually declined. We have reported peak lightning at 15:00 UTC with the highest FR upto 1661 flashes $hour^{-1}$. The Morrison successfully captured the peak lightning at 15:00 UTC with 2238 flashes $hour^{-1}$ and overestimation of 577 flashes $hour^{-1}$. Thomson, WDM5 and WSM6 also captured the peak lightning closely with a lead time of 1–2 hours as compared to ILLN. In the decay phase, Thompson and WDM5 showed trends like those of WSM6 and Morrison. Furthermore, we have applied cross-correlation analysis to identify the lead-leg pair with the highest correlation. WSM6 and WDM5 show 3 hours lead with high ($r = 0.76$ & 0.80) correlations, and Thompson and Morrison show only 1 hourly lead, with slightly lower correlation ($r = 0.73, 0.60$). Vani et al. (2022) reported notable FSS for lightning activity over the WG, and also reported instances of both overestimation and underestimation. For example, in 81.25% of the cases, the model showed a lead or lag of 1–3 hours and in 18.75% of cases, the shift was up to 6 hours.

3.3 Spatial and longitudinal variations

Figure 4 depicts the intercomparison between the model simulated and ILLN observed FR spatial distribution. As the two platform have different range of variations, for a more meaningful comparison, we have calculated the Normalized Flash Rate (NFR). The NFR is derived by converting flash points into 3 km grids and then dividing by the maximum FR. The ILLN observations indicate the accumulation of high NFR (0.8 to 1.0) over the foothills of the Himalayas in Himachal Pradesh, Uttarakhand, northern Uttar Pradesh and Nepal as described in Fig. 4a (Kumar et al. 2024; Gautam et al. 2022). The WSM6 captures lightning activity over the foothills but weakly captured NFR over south-eastern region. However, it effectively rejected non-lightning events (Fig. 4b). The Thompson MP scheme captures slightly more lightning activity over the foothills with fewer false detection as shown in Fig. 4c. It should be noted that, Morrison detects more lightning event but suffers from false detection and comparatively fails to reject non-lightning events (Fig. 4d). The WDM5 also captures lightning activity better as compared to the WSM6 across the entire foothill region, however, generates a significant false detection (Fig. 4e). Overall, all MP schemes demonstrate the ability to reject non-lightning events and identify lightning hotspots.

To understand the shift in lightning distribution, we plotted the average longitudinal variation (Fig. 4f). The MP schemes showed overestimation compared to the ILLN between 75° to 77°E and Thompson showed the least longitudinal deviation (only 0.27°E) from the observed lightning peak. The WSM6 had a deviation of 0.58°E and aligned well with observations, producing stable results. However, the Morrison and WDM5 showed larger deviations ranging from 2.95° to 3.19°E, suggesting significantly high overestimation. Recently, Mohan et al. (2021) reported strong agreement between ILLN and simulated FR with a high spatial correlation of 82.7%. Similarly, Vani et al. (2022) reported that WDM5 performed better than Thompson with a spatial shift in isolated lightning events over WG region. The more details of spatial performance of MP schemes have also discussed in section 3.7–3.8.

3.4 Evolution of simulated convective parameters

Convection plays a critical role in cloud microphysical processes and lightning generation. Convective Available Potential Energy (CAPE) serving as a key indicator of convective activities (Kamra and Kumar, 2020). We have examined the dynamics of simulated CAPE at 850 hPa during the initial, active, and dissipation phases (Fig. S2). During initial phase, low CAPE (< 250 Jkg^{-1}) dominates the most region, but due to localized convective high convection zones (HCZ) particularly over Rajasthan, Haryana, Punjab, and Uttar Pradesh and show relatively high CAPE (< 750 Jkg^{-1}). During the active phase, most of the region is covered by moderate CAPE (250–750 Jkg^{-1}) and HCZ exhibits high CAPE (750 and > 2000 Jkg^{-1}). The Morrison and WDM5 well simulate the convection activities, and WDM5 reflects efficient transition phases. However, isolated small convective pockets can still support lightning. The Decay phase also depicts localized high convection, but stability dominates the region (< 250 Jkg^{-1}). The spatial and temporal patterns of simulated CAPE align well FR (Figs. 3 and 4). In the WHR, especially over the higher-elevation regions, CAPE may not be a primary contributor for lightning activity and show lead relation with lightning FR density (Kumar et al. 2024; r = 0.34). Conversely, lightning in the NW Himalayan

foothills is largely driven by solar heating, precipitable water, cloud clustering and orographic uplift (Kamra and Kumar, 2020). So, foothills may contribute to the initiation of the strong convection (surface-based convective lifting), and hilly terrain redistributes them, where orographic lifting may be important (Biswasharma 2025a, c).

3.5 Cloud microphysical properties

The MP scheme plays a crucial role in governing lightning activity, interaction between graupel and cloud ice particles through collisions enhances cloud electrification, ultimately leading to severe lightning (Adamo et al. 2007; Yair et al. 2010; Hazra et al. 2013; Williams et al. 2002; Choudhury et al. 2020). Therefore, understanding and evaluation of MP schemes are essential for improving lightning prediction and representing in the model. In the present study, we have investigated the temporal and vertical distribution of Cloud Water Mixing Ratio (q_c), Rainwater Mixing Ratio (q_r), Snow Mixing Ratio (q_s), and Ice Mixing Ratio (q_i) simulated over the domain (Figs. 5–6). The q_c has a significant contribution in lightning activity, as the presence of high q_c indicates more supercooled liquid droplets available for hydrometeor growth (Bovalo et al. 2019). Updraughts transport these droplets to higher altitudes, facilitating the conversion into ice and snow particles through the Wegener-Bergeron-Findeisen process (WBFP) in mixed phase region (MPR) of thundercloud (Storelvmo & Tan, 2015). The time-height variations of the domain-averaged q_c obtained from different MP schemes are presented in Fig. 5(i). The q_c shows a significant vertical extent between 5.5 and 8.5 km, which can be converted into ice and snow particles via accretions and riming process (Korolev, 2007). The presence of hydrometeor significantly contributes to charge separation (Mansell et al. 2005). Thompson and Morrison show stronger evidence of elevated q_c ($> 2.5 \times 10^{-5}$ kg kg^{-1}) and correspond well with FR variation during the active phase (Figs. 5(i)b & 5(i)c). The WSM6 and WDM5 also generate high q_c levels $> 2.5 \times 10^{-5}$ kg kg^{-1} during active phase (Figs. 5(i)a, d), with scattered q_c structures and coinciding with FR trend (Fig. 3). Which is indicating the favourable condition for the hydrometeor growth, charge separation, electrification and lightning.

The q_r simulation shows significantly high values (5×10^{-5} kg kg-^{1}) between active phase with a vertical extent from the surface up to 4 km in the WSM6, Thompson, and WDM5 (Fig. 5(ii) a, b & d). In contrast, the Morrison exhibits peak q_r during the decay phase, with maximum values exceeding 2.5×10^{-5} kg kg-^{1} (Fig. 5(ii)c). The presence of high q_r values in active phase suggesting the collision and coalescence processes to initiate the warm rain processes (WRP) in shallow MPR later at 15 UTC (Rosenfeld and Lensky 1998). The effect of WRP in thunderstorm has been observed and it is dissipating due to significant contribution of downdraughts generated by dominance of high gridded average rainfall up to 1.3 mm at 18 UTC as observed by the GPM observations.

The q_s clearly indicates dominance during both the active and decay phases of FR, with significant vertical extension from 4–14 km (Fig. 6a-d). The Thompson and WDM5 microphysics exhibit high q_s values exceeding 7.5×10^{-5} kg kg-^{1} within MPR and above MPR between 5.5 and 12 km well as shown in

the Fig. 6(i)b, d. A high snow content zone persists for several hours (11–21 UTC), suggesting active depositional growth and riming, which are crucial for graupel and snow production, ultimately leading to severe lightning. It should be noted that, in Thompson MP ice is transfer to the snow therefore Thompson shows relatively high snow but weak ice production (Ko et al. 2022). Furthermore, Choudhury et al. (2020) highlighted that snow formation is affected by strong updraughts, induced by latent heat release and regulates auto-conversion of cloud ice to snow at high altitudes. Which support the riming process, charge segregation, cloud electrification and thus contribute severe lightning. However, the WSM6 and Morrison show relatively lower snow production (Fig. 6(i)a, c).

Figure 6(ii)a-d describes the q_i, which is a crucial hydrometeor for understanding the microphysical characteristics of ice-phase cloud development and its role in subsequent precipitation and lightning generation. The WSM6, Morrison, and WDM5 shows a widespread and elevated $q_i > 2.5 \times 10^{-5}$ kg kg^{-1} between approximately 8–12 km altitude. The Morrison exhibits a broader peak with highest q_i upto 5×10^{-5} kg kg^{-1} between 9–13 km, suggesting active ice production and dominance of cold cloud processes. However, this enhanced ice-phase development does not directly translate to strong surface rainfall, possibly due to weak WRP. The weakest q_i is generated by the Thompson as compared to WSM6 and WDM5 MP Schemes. Weak ice production in Thompson MP schemes is due to generation of relatively smaller ice particles (Ko et al. 2020; Bao et al. 2021). Understanding such critical differences is crucial for improving cloud microphysics, cloud-radiation interactions, thunderstorm dynamics. Several past studies support these observations, Hazra et al. (2013) investigated the role of cloud ice in lightning and heavy rainfall using WRF simulations and in-situ measurements from an ice nuclei spectrometer. They found that the Fletcher, 1962 or F1962 MP scheme generated hydrometeors more favourable for lightning (Fletcher, 1962). Similarly, Unnikrishnan et al. (2021) reported a strong spatial analogy between cloud ice water content and lightning frequency over the NE and NW Indian regions. The vertical moisture transport, combined with the WBFP and cold cloud processes initiates the growth of hydrometeors and condensational latent heat release. Which strengthens the further vertical updraughts and cloud development for severe lightning generation (Korolev, 2007; Hazra et al. 2013; Choudhury et al. 2020). Likewise, Biswasharma et al. (2021) highlighted the dominance of high concentrations of ice particle during thunderstorms over Rampurhat compared to Nagaland. In our study, the existence of hydrometeors reinforces the critical role in shaping severe lightning episodes over WHR.

3.6 Temporal evaluation of lightning

The temporal performance of MP schemes has been evaluated by employing Taylor diagrams, which provide critical performance statistics such as correlation coefficient (r), standard deviation (SD), and root mean square error (RMSE) etc. (Taylor et al. 2001; Federico et al. 2022; Yadava et al. 2023; Biswasharma et al. 2024). Among MP schemes, Thompson indicates most favourable performance characteristics due to high (r = 0.63) and balance RMSE (429 flashes $hour^{-1}$) between ILLN observation and model generated FR. It means, Thompson successfully generates comparable magnitude and temporal behaviour of ILLN observed FR (Fig. 7(i)). Morrison shows highest RMSE (518 flashes $hour^{-1}$) with a lower correlation (r = 0.53), which is indicating overestimation as compared to the observation.

The WSM6 shows lowest performance characteristics, displaying slightly lower RMSE (458.2 flashes $hour^{-1}$) and weak correlation (r = 0.34), with performance metrics closely similar to WDM5 (r = 0.43, RMSE: 448.8 flashes $hour^{-1}$). Overall, Thompson demonstrates better skill, Morrison shows a reasonable correlation despite higher RMSE. Both WSM6 and WDM5 suggest similar, but weaker lightning simulation capabilities in temporal evaluation over WHR (Fig. 7(i)).

The spatial performance evaluation of the MP schemes has been carried out by preparation of spatial contingency table for each 12 km, 21 km and 51 km grid and then FSS has been computed over TD domain. The POD show increasing trend towards larger grid and MP schemes are producing stable results with low FAR and Bais. We have observed that Morrison had the highest detection skill (POD = 0.66, CSI = 0.39, Accuracy = 0.55), but it slightly overpredicted (Bias = 1.01) and suffers from high FAR (0.55) in 12 km grid (Fig. 7(ii)a). WSM6, Thompson and Morrison show slightly better performance at 21 km grid in terms of POD, CSI, Accuracy. But due to low FAR and Bais, WDM5 shows slightly better Accuracy as shown in Fig. 7(ii)b. In the largest 51 km grid, the performance of MP schemes shows significant enhancement. For example, Thompson, Morrison, WDM5 and WSM6 show high POD (0.82, 0.84, 0.81 & 0.78), CSI (0.72, 0.64, 0.69, 0.64), accuracy (0.76, 0.65, 0.73, 0.68) and low FAR (0.13, 0.26, 0.17) and Bias (0.95, 1.15, 0.98, 0.94) respectively (Fig. 7(ii)c). Therefore, Thompson can predict the FR well while maintaining the lowest FAR and Bias over TD. Although Morrison has high POD, it has significant overestimation and high FAR with low Accuracy and CSI. The spatial performance of the MP Schemes also depends upon the grid resolution. For example, Vani et al. (2022) have selected sixteen lighting cases over the Maharashtra and evaluated the model performance. They have reported high FSS in 50 km grid in comparison with 10 km grid. Similarly, Kumar et al. (2022, 2023) have simulated the extreme cases of lightning over the Bihar and Rajasthan and evaluated the WRF model performance. They observed POD is in the range of 0.5–0.69 by using different combinations of parameterization schemes. The FSS of our analysis in case of all MP schemes is comparable with these previous studies.

3.7 Spatial and temporal evaluation of rainfall

Several studies have reported strong spatial and temporal associations between rainfall and lightning over different regions (Lal and Pawar, 2009; Petersen and Rutledge, 1998; Williams et al. 1992). In this context, we have also evaluated the model performance to examine whether microphysics schemes that perform well for the lightning prediction can exhibit similar skill for rainfall, or whether different model configurations and tuning are required to represent both the processes. The spatial and temporal performance of the model for predicting rainfall in comparison with GPM derived grid average rainfall shown in Fig. 8(i). In temporal performance, GPM data shows a high SD (0.36 mm) as compared to the model simulated rainfall (0.02–0.3 mm). WSM6 shows the highest correlation (r = 0.74) with GPM data, while Thompson (r = 0.52) and Morrison (r = 0.45) show moderate correlations. WDM5 shows the lowest correlation (r = 0.26) with lowest SD (0.02 mm). It is to be noted that Thomson and Morrison schemes show the best performance for lightning simulation but not for rainfall over TD.

The evaluation of spatial performance using FSS for four different thresholds (0.1 mm, 0.5 mm, 1 mm, and 2 mm) of rainfall, has been carried out at grid resolution of 12 km as shown in Fig. 8(ii). The WSM6, Thompson, Morrison and WDM5 MP schemes were able to predict (0.1 mm threshold) rainfall with moderate to low POD (0.64, 0.37, 0.29, 0.25) and low FAR (0.02–0.04) as shown Fig. 8(ii)a. The Morrison shows the highest Accuracy (0.63) but with high bias (0.68) at 0.1 mm threshold. Furthermore, we observed that the POD and CSI are decreasing while FAR is increasing from 0.1 to 2 mm threshold. It means that model could not capture rainfall at a higher threshold over the TD domain (Fig. 8(ii)). In both lightning and rainfall, Morrison shows high POD but suffers from the FAR and Bais issues (Fig. 7(ii), 8(ii)). Navale and Singh (2020) have explored the influence of topography on the performance of the WRF model for simulation of rainfall compared with IMD GPM over the NW Himalayan region, particularly over Uttarakhand and Himachal Pradesh. They found that WRF model simulates the rainfall well with considerable FSS such as Hit Rate (0.78–0.85), FAR (0.20–0.42), accuracy (0.70 – 0.60), CSI (0.70 – 0.52) for 0.1 mm threshold. Overall, WSM6 showed relatively better performance in capturing temporal variations while Morrison showed higher FSS for spatial variations. We noted that for lightning simulation, Morrison and Thompson consistently performed better than the other schemes. Consequently, no single microphysics scheme emerges as uniquely superior for simulating both rainfall and lightning, indicating scheme-dependent performance across processes.

The vertical profiles of domain-averaged q_c, $q_{r,}$ q_{sa} and q_i simulated using four MP schemes during the active phase of the thunderstorm shown in Fig. 9(i)a-d. All MP schemes show high q_c between 3–5 km; however, Thompson and Morrison schemes maintain relatively higher q_c and a deeper vertical extent reaching to mid-troposphere (5–8 km). This indicates that more supercooled liquid water stays higher in the cloud, which is essential for non-inductive charge separation through graupel-ice interactions (Takahashi, 1978; Tsenova and Mitzeva 2008). The WSM6 and WDM5 schemes produce shallow cloud water profiles, which favor faster conversion to precipitation. The q_r peaks in the lower troposphere (2–4 km) across all schemes, but Morrison shows comparatively stronger rainwater production and a more coherent vertical structure near the surface. This suggests efficient warm-rain processes and rapid conversion of cloud water into rain causing high surface rainfall (King et al. 2015). In contrast, Thompson scheme shows decreasing rainwater, consistent with delayed precipitation formation due to prolonged liquid water retention aloft. q_s dominate above ~ 6 km, with Thompson scheme showing high q_s within the MPR. This increase in snow mass indicates active depositional growth and riming processes, which are closely linked to graupel formation and lightning electrification. The WSM6 scheme shows relatively lower snow aloft, reflecting weaker cold-cloud microphysical processes. The q_i reveals marked scheme-dependent differences. The Thompson scheme produces slightly less but more uniform ice distribution due to a smaller ice particle spectrum within the MPR (Bao et al. 2021). The WSM6 scheme shows comparatively extensive ice profiles, consistent with its single-moment formulation and emphasis on precipitation efficiency rather than electrification. Overall, the vertical hydrometeor profiles indicate that Thompson, Morrison scheme increases mixed-phase processes which are critical for lightning generation, whereas WSM6 scheme favors efficient warm-rain production and surface rainfall.

Figure 9(ii)a-d presents Contoured Frequency by Altitude Diagrams (CFADs) of simulated reflectivity, highlighting pronounced differences in storm vertical structure across microphysics schemes. WSM6 scheme shows high-frequency reflectivity exceeding 40 dBZ primarily below ~ 4 km, indicating efficient warm-rain processes and strong rainfall production, but weaker mixed-phase development aloft. In contrast, Thompson scheme shows moderate-to-high reflectivity extending coherently into the mixed-phase region (5.5–8.5 km), indicating active riming and graupel growth, which are favorable for charge separation and lightning generation. Morrison scheme shows large spread in reflectivity, supporting precipitation growth but with less organized mixed-phase structure, while WDM5 shows intermediate behavior. These differences demonstrate that the choice of microphysics strongly controls storm structure, with Thompson scheme favoring lightning-related processes while WSM6 scheme emphasizing rainfall production.

Overall, the evaluation indicates that the WRF-simulated lightning and rainfall are substantially sensitive to the choice of MP scheme. The Thompson scheme shows better temporal skill for lightning, while Morrison performs better in spatial detection, and WSM6 captures rainfall variability more effectively. However, no single scheme consistently outperforms best for both lightning and rainfall, highlighting that WRF simulations are not uniformly reliable across processes. These contrasting performances underscore the need for further targeted tuning and region-specific optimization of model physics for improved simultaneous simulation of lightning and precipitation over complex terrain. The contrasting performance of microphysics schemes for lightning and rainfall arises from fundamental differences in how they represent mixed-phase cloud processes, hydrometeor growth, and precipitation conversion. Lightning production is strongly controlled by the coexistence of supercooled liquid water, graupel, and ice within the mixed-phase region, which promotes non-inductive charge separation through riming and collisions (Takahashi, 1978; Saunders, 2008; Williams et al. 2002). Schemes such as Thompson, which incorporate more detailed ice-phase physics and riming processes, tend to sustain hydrometeors within the charging zone for longer durations, thereby enhancing electrification and lightning activity (Thompson et al. 2008; Morrison et al. 2009; Choudhury et al. 2020). In contrast, rainfall simulation is more sensitive to warm-rain processes, auto-conversion rates, and melting efficiency, which are emphasized in simpler bulk schemes such as WSM6, leading to more efficient precipitation production near the surface (Hong and Lim, 2006; Halder and Mukhopadhyay, 2016; Kumar et al. 2023). As a result, schemes optimized for electrification processes do not necessarily maximize rainfall skill, and vice versa. Similar scheme-dependent behavior has been reported in earlier WRF-based lightning and precipitation studies over India and other convective regions (Mohan et al. 2021; Vani et al. 2022; Kumar et al. 2022; Haldar and Mukhopadhyay 2016), highlighting that no single microphysics formulation can simultaneously optimize both lightning and rainfall simulations, particularly over complex terrain.

It is to be noted that the analysis is based on a single severe pre-monsoon lightning event, and therefore, the results may not be fully representative of the wide range of convective environments and storm types that occur over the western Himalaya. Model performance and microphysics sensitivity may vary under different synoptic conditions, seasons, and storm intensities. In addition, uncertainties associated with lightning parameterization, observational detection efficiency, and model resolution over complex terrain

can influence the results. Future studies using a larger sample of events across multiple seasons and regions are needed to generalize the findings and further refine model physics for improved lightning and rainfall simulations.

4 Conclusion

This study examined a severe pre-monsoon lightning event over the complex terrain of WHR on 23 May 2023 and evaluated the ability of the WRF model to simulate lightning and associated convective processes using four MP schemes (WSM6, Thompson, Morrison, and WDM5). Lightning simulations were evaluated against ILLN observations, while rainfall was assessed using GPM observations. The analysis focused on temporal evolution, spatial distribution, thermodynamical and microphysical characteristics. All MP schemes captured the broad temporal evolution of lightning activity, including the initial, active, and decay phases, but differed significantly in magnitude, timing, and variability. Morrison reproduced the timing of peak FR but with overestimated magnitude, whereas the Thompson scheme showed the closest agreement with observed lightning variability with reduced false detections. WSM6 and WDM5 showed larger timing offsets and higher variability. A pronounced increase in CAPE occurred from the initial phase (< 250 J kg^{-1}) to the active phase (250–750 J kg^{-1}) of thunderstorm, with some zones exceeding 2000 J kg^{-1}. Morrison effectively captured this transition. During the active phase, Thompson and Morrison simulated enhanced mid-level cloud water ($q_c \gtrsim 2 \times 10^{-5}$ kg kg^{-1}) between 4–8 km, supporting sustained updrafts and latent heat release. Elevated snow mixing ratios ($q_s \gtrsim 7 \times 10^{-5}$ kg kg^{-1}) extending into the mixed-phase region indicated active depositional and riming growth favorable for lightning. In contrast, WSM6 produced stronger low-level rainwater peaks ($q_r \gtrsim 5 \times 10^{-5}$ kg kg^{-1} below ~ 4 km), reflecting efficient WRP and enhanced surface precipitation during the decay phase of thunderstorm. These contrasting hydrometeor profiles explain the divergent performance of MP schemes for simulating lightning and rainfall. Schemes that retain supercooled liquid water and ice in the MPR favour charge separation and lightning, whereas schemes emphasizing rapid WRP enhances surface rainfall but limits electrification. Consequently, no single MP scheme consistently outperforms others for both lightning and rainfall over the WHR.

Overall, WRF performance over the complex Himalayan terrain is strongly process- and scheme-dependent, indicating that microphysics configurations optimized for one atmospheric process may not be transferable to others. The contrasting behavior of MP schemes for lightning and rainfall highlights the need to treat electrification and precipitation as distinct yet interacting outcomes of storm microphysics, rather than assuming a single optimal setup. These findings have important implications for high-impact weather prediction over mountainous regions, where lightning, cloudbursts, and intense rainfall frequently co-occur. Improving model reliability therefore requires region-specific and process-aware tuning of microphysics schemes, guided by detailed observational evaluation. More broadly, the results emphasize that robust lightning prediction must be grounded in physically consistent representations of mixed-phase cloud processes, which are also relevant to other orographically influenced convective environments.

Declarations

Declarations Competing of interest: The authors declare that they have no financial or personal relationships that could have influenced the work reported in this manuscript.

Use of AI Tools

The authors used an AI-based language editing tool to improve the grammar, clarity, and readability of the manuscript. The AI tool was not used for scientific interpretation, data analysis, figure preparation, or the generation of research content. All scientific conclusions, analyses, and interpretations were developed and verified by the authors.

Funding

Not Applicable

Author Contribution

Sanjeev Kumar: Conceptualization, Data curation, Formal analysis, Methodology, Software, Writing-original draft, Writing-review & editing. N. Umakanth: Data curation, Formal analysis, Methodology, Software. Alok Sagar Gautam: Conceptualization, Investigation, Project administration, Validation. Rupraj Biswasharma: Conceptualization, Investigation, Methodology, Validation, Visualization, Writing-original draft, Writing-review & editing. Swapnil S. Potdar: Data curation, Methodology, Software, Writing-review & editing. Karan Singh: Data curation, Software. Devendraa Siingh: Investigation, Project administration, Resources, Supervision, Validation. R. P. Singh: Visualization, Writing - original draft.

Acknowledgement

Indian Institute of Tropical Meteorology, Pune, is funded by the Ministry of Earth Sciences, Government of India. We are sincerely thankful to Head of the Department of Physics; and the Vice-Chancellor of Hemvati Nandan Bahuguna Garhwal University, Srinagar, for providing the support and infrastructure necessary for this research. We gratefully acknowledge the data providers and modelling platforms that supported this study, including the Global Hydrometeorology Resource Center (GHRC), the European Centre for Medium-Range Weather Forecasts (ECMWF), NASA's Giovanni portal, and the National Centers for Environmental Prediction (NCEP) team, whose resources were crucial to the analysis and outcomes of this work.

Data availability

The Weather Research and Forecasting (WRF) Model version 4.5 used in this study is publicly available from NCAR at https://www.mmm.ucar.edu/models/wrf and via the official GitHub repository at https://github.com/wrf-model/WRF/tree/release-v4.5. Lightning observations from the Indian Lightning Location Network (ILLN) are available upon reasonable request, subject to institutional data policies. The dataset supporting this study is publicly available at Zenodo (Kumar et al. 2026). The archived dataset includes lightning flash grids, rainfall time series, vertical hydrometeor profiles, and spatial rainfall fields used for model evaluation. The data can be accessed at https://doi.org/10.5281/zenodo.18747188

References

1. Adamo C, Solomon R, Medaglia CM, Dietrich S, Mugnai A (2007) Cloud Microphysical Properties from Remote Sensing of Lightning within the Mediterranean. Measuring Precipitation From Space: EURAINSAT and the Future. Springer Netherlands, Dordrecht, pp 127–134. ttps://doi.org/10.1007/978-1-4020-5835-6_10
2. Agnihotri CL, Singh MS (1982) Satellite study of western disturbances. Mausam 332:249–254. ttps://doi.org/10.54302/mausam.v33i2.3254
3. Bao J, Michelson S, Grell E (2021) Uncertainties in the parameterization of cloud microphysics: An illustration of the problem. Uncertainties in Numerical Weather Prediction, Elsevier, pp. 265–296. ttps://doi.org/10.1016/b978-0-12-815491-5.00010-0
4. Berdeklis P, List R (2001) The Ice Crystal-Graupel collision charging mechanism of thunderstorm electrification. J Atmos Sci 58:2751–2770. ttps://doi.org/10.1175/1520-0469(2001)058
5. Biswasharma R, Domkawale MA, Ghosh R, Gangane A, Umakanth N, Kumar S, Gopalakrishnan V, Pawar SD, DiGangi E, Deshpande SM, Samanta D, Sharma S (2025b) Assessment of the Indian Lightning Location Network (ILLN) using ground-based and satellite observations. Atmos Res 320:108069. ttps://doi.org/10.1016/j.atmosres.2025.108069
6. Biswasharma R, Pramanik GP, Umakanth N, Longkumer I, Pongener I, Konwar M, Debajyoti S, Lal DM, Gopalakrishnan V, Pawar SD, Kamra AK, Sharma S (2025c) Evaluating thunderstorm characteristics and air quality during the COVID-19 lockdown in Northeastern and Eastern India. Atmos Res 320:108053. ttps://doi.org/10.1016/j.atmosres.2025.108053
7. Biswasharma R, Roy P, Imolemba N, Imlisunup N, Samanta D, Pramanik GP, Sharma S (2021) Regional variation of electrical and lightning properties of thunderclouds during the premonsoon season over the north-eastern and eastern part of India. Atmos Res 260:105683. ttps://doi.org/10.1016/j.atmosres.2021.105683
8. Biswasharma R, Umakanth N, Pongener I, Longkumer I, Rao KMM, Pawar SD, Gopalkrishnan V, Sharma S (2024) Sensitivity analysis of cumulus and microphysics schemes in the WRF model in simulating Extreme Rainfall Events over the hilly terrain of Nagaland. Atmos Res 304:107393. ttps://doi.org/10.1016/j.atmosres.2024.107393
9. Biswasharma R, Pongener I, Longkumer I, Satyanarayana G, Ch, Pawar SD, Gopalakrishnan V, Sharma S (2025a) Simulation of premonsoon thunderclouds over two climatic regimes: Evaluation

and dichotomous detection. Atmos Res 320:108027. ttps://doi.org/10.1016/j.atmosres.2025.108027

10. Blakeslee R (2019) Quality Controlled Lightning Imaging Sensor (LIS) on International Space Station (ISS) science data [Dataset]. In Earth Observing System Data and Information System. ttps://doi.org/10.5067/lis/isslis/data108
11. Boccippio DJ (2002) Lightning scaling relations revisited. J Atmos Sci 59:1086–1104. ttps://doi.org/10.1175/1520-0469(2002)059
12. Bookhagen B, Thiede RC, Strecker MR (2005) Abnormal monsoon years and their control on erosion and sediment flux in the high, arid northwest Himalaya. Earth Planet Sci Lett 231:131–146. ttps://doi.org/10.1016/j.epsl.2004.11.014
13. Bovalo C, Barthe C, Pinty J (2019) Examining relationships between cloud-resolving model parameters and total flash rates to generate lightning density maps. Q J R Meteorol Soc 145:1250–1266. ttps://doi.org/10.1002/qj.3494
14. Choudhury BA, Konwar M, Hazra A, Mohan GM, Pithani P, Ghude SD, Deshamukhya A, Barth MC (2020) A diagnostic study of cloud physics and lightning flash rates in a severe premonsoon thunderstorm over northeast India. Q J R Meteorol Soc 146:1901–1922. ttps://doi.org/10.1002/qj.3773
15. Chowdhury Ghoshal S, Ganguly D, Khan AW, Dey S (2025) Aerosol-Cloud Interactions and Their Role in Modulating Lightning Activity: Evidence From Extreme Events Over India. J Geophys Res Atmos 130. ttps://doi.org/10.1029/2024JD043251. e2024JD043251
16. Cooper MA, Holle RL (2018) Current global estimates of lightning fatalities and injuries. Springer Natural Hazards. Springer, Cham 65–73. ttps://doi.org/10.1007/978-3-319-77563-0_6
17. Dafis S, Fierro A, Giannaros TM, Kotroni V, Lagouvardos K, Mansell E (2018) Performance evaluation of an explicit lightning forecasting system. J Geophys Res Atmos 123:5130–5148. ttps://doi.org/10.1029/2017jd027930
18. De Meij A, Ojha N, Singh N, Singh J, Poelman DR, Pozzer A (2022) The impact of High-Resolution SRTM topography and corine land cover on lightning calculations in WRF. Atmos 13:1050. ttps://doi.org/10.3390/atmos13071050
19. Dimri AP, Immerzeel WW, Salzmann N, Thayyen RJ (2017) Comparison of climatic trends and variability among glacierized environments in the Western Himalayas. Theor Appl Climatol 134:155–163. ttps://doi.org/10.1007/s00704-017-2265-8
20. Federico S, Torcasio RC, Lagasio M, Lynn BH, Puca S, Dietrich S (2022) A Year-Long Total Lightning Forecast over Italy with a Dynamic Lightning Scheme and WRF. Remote Sens 14:3244. ttps://doi.org/10.3390/rs14143244
21. Gangane A, Priyadarshini P, Pawar SD, Syed HA, Biswasharma R, Gopalakrishnan V, Lal DM (2025) Falling trend of winter lightning over Western India and its possible relation with Western disturbances. Earth Space Sci 12:e2024EA003726. ttps://doi.org/10.1029/2024ea003726

22. Gautam AS, Joshi A, Chandra S, Dumka UC, Siingh D, Singh RP (2022) Relationship between Lightning and Aerosol Optical Depth over the Uttarakhand Region in India: Thermodynamic Perspective. Urban Sci 6:70. ttps://doi.org/10.3390/urbansci6040070
23. Gautam MR, Timilsina GR, Acharya K (2013) Climate change in the Himalayas: Current state of knowledge. World Bank. ttps://doi.org/10.1596/1813-9450-6516. Washington, DC eBooks
24. Giannaros TM, Kotroni V, Lagouvardos K (2015) Predicting lightning activity in Greece with the Weather Research and Forecasting (WRF) model. Atmos Res 156:1–13. ttps://doi.org/10.1016/j.atmosres.2014.12.009
25. Halder M, Mukhopadhyay P (2016) Microphysical processes and hydrometeor distributions associated with thunderstorms over India: WRF (cloud-resolving) simulations and validations using TRMM. Nat Hazards 83:1125–1155. ttps://doi.org/10.1007/s11069-016-2365-2
26. Halder M, Hazra A, Mukhopadhyay P, Siingh D (2015) Effect of the better representation of the cloud ice-nucleation in WRF microphysics schemes: A case study of a severe storm in India. Atmos Res 154:155–174. ttps://doi.org/10.1016/j.atmosres.2014.10.022
27. Hazra A, Goswami BN, Chen J (2013) Role of Interactions between Aerosol Radiative Effect, Dynamics, and Cloud Microphysics on Transitions of Monsoon Intraseasonal Oscillations. J Atmos Sci 70:2073–2087. ttps://doi.org/10.1175/jas-d-12-0179.1
28. Hong S, Noh Y, Dudhia J (2006) A New Vertical Diffusion Package with an Explicit Treatment of Entrainment Processes. Mon Weather Rev 134:2318–2341. ttps://doi.org/10.1175/mwr3199.1
29. Hunt KMR, Baudouin J, Turner AG, Dimri AP, Jeelani G, Chattopadhyay R, Cannon F, Arulalan T, Shekhar MS, Sabin TP, Palazzi E (2025) Western disturbances and climate variability: a review of recent developments. Weather Clim Dyn 6:43–112. ttps://doi.org/10.5194/wcd-6-43-2025
30. Iacono MJ, Delamere JS, Mlawer EJ, Shephard MW, Clough SA, Collins WD (2008) Radiative forcing by long-lived greenhouse gases: Calculations with the AER radiative transfer models. J Geophys Res Atmos 113:D13103. ttps://doi.org/10.1029/2008jd009944
31. India T (2023) https://www.indiatoday.in/india/story/24-goats-struck-dead-by-lightning-in-uttarakhand-2383550-2023-05-25
32. Kamra AK, Kumar PR (2020) Regional variability in lightning activity over South Asia. Int J Climatol 41:625–646. ttps://doi.org/10.1002/joc.6641
33. Kashyap A, Behera MD (2023) The influence of landslide morphology on erosion rate variability across western Himalayan catchments: Role of westerlies and summer monsoon interaction in the landscape characterization. Geol J 59:1112–1125. ttps://doi.org/10.1002/gj.4913
34. King JM, Kummerow CD, Van Den Heever SC, Igel MR (2015) Observed and Modeled Warm Rainfall Occurrence and Its Relationships with Cloud Macrophysical Properties. J Atmos Sci 72:4075–4090. ttps://doi.org/10.1175/jas-d-14-0368.1
35. Ko J, Lim KS, Kim K, Lee G, Thompson G, Berne A (2022) Simulated microphysical properties of winter storms from bulk-type microphysics schemes and their evaluation in the Weather Research

and Forecasting (v4.1.3) model during the ICE-POP 2018 field campaign. Geosci Model Dev 15:4529–4553. ttps://doi.org/10.5194/gmd-15-4529-2022

36. Korolev AV, Isaa GA, Strapp JW, Cober SG, Barker HW (2007) In situ measurements of liquid water content profiles in midlatitude stratiform clouds. Q J R Meteorol Soc 133:1693–1699. ttps://doi.org/10.1002/qj.147
37. Kumar A, Das S, Panda S (2022) Numerical simulation of a widespread lightning event over north India using an ensemble of WRF modeling configurations. J Atmos Sol-Terr Phys 241:105984. ttps://doi.org/10.1016/j.jastp.2022.105984
38. Kumar A, Panda SK, Mondal U, Sharma D, Das S (2023) Assessment of model time step and domain resolution of WRF model to simulate the lightning over Bihar and Rajasthan, India. Model Earth Syst Environ 9:3959–3984. ttps://doi.org/10.1007/s40808-023-01724-3
39. Kumar PR (2017) Lightning, rainfall, AOD, and convection variabilities in the monsoon zone of India. Int J Remote Sens 39:727–740. ttps://doi.org/10.1080/01431161.2017.1392636
40. Kumar S, Biswasharma R, Potdar SS, Siingh DS (2026) Data for: Evaluation of WRF microphysics schemes for simulating lightning and rainfall over the complex terrain of the western Himalayan region [Dataset]. ttps://doi.org/10.5281/zenodo.18747188. Zenodo
41. Kumar S, Gautam AS, Kamra AK, Singh K, Potdar SS, Siingh D (2024) Lightning distribution and its association with surface thermodynamics parameters over a western Himalayan region. J Earth Syst Sci 133:234. ttps://doi.org/10.1007/s12040-024-02406-z
42. Lal DM, Pawar SD (2009) Relationship between rainfall and lightning over central Indian region in monsoon and premonsoon seasons. Atmos Res 92:402–410. ttps://doi.org/10.1016/j.atmosres.2008.12.009
43. Latham J, Mason BJ (1962) Electrical charging of hail pellets in a polarizing electric held. Proc R Soc Lond A 266:387–401. ttps://doi.org/10.1098/rspa.1962.0068
44. Lim KSS, Hong SY (2010) Development of an Effective Double-Moment Cloud Microphysics Scheme with Prognostic Cloud Condensation Nuclei (CCN) for Weather and Climate Models. Mon Weather Rev 138:1587–1612. ttps://doi.org/10.1175/2009MWR2968.1
45. Lin Y, Fan J, Jeong J, Zhang Y, Homeyer CR, Wang J (2020) Urbanization-Induced land and aerosol impacts on storm propagation and hail characteristics. J Atmos Sci 78:925–947. ttps://doi.org/10.1175/jas-d-20-0106.1
46. Lohan N, Routray A, Kumar R, Mahala BK, Kumar S (2025) Validation and diagnostic study of cloudburst events over the Himalayan region using IMDAA and ERA5. Geomat Nat Hazards Risk 16. ttps://doi.org/10.1080/19475705.2024.2446589
47. Lund NR, MacGorman DR, Schuur TJ, Biggerstaff MI, Rust WD (2009) Relationships between Lightning Location and Polarimetric Radar Signatures in a Small Mesoscale Convective System. Mon Weather Rev 137:4151–4170. ttps://doi.org/10.1175/2009MWR2860.1
48. Mansell ER, MacGorman DR, Ziegler CL, Straka JM (2005) Charge structure and lightning sensitivity in a simulated multicell thunderstorm. J Geophys Res Atmos 110:12101.

ttps://doi.org/10.1029/2004JD005287

49. Mishra M, Acharyya T, Guria R et al (2024) Lightning-related fatalities in India (1967–2020): a detailed overview of patterns and trends. Environ Dev Sustain. ttps://doi.org/10.1007/s10668-024-05276-z
50. Mohan GM, Vani KG, Hazra A, Mallick C, Chaudhari HS, Pokhrel S, Pawar S, Konwar M, Saha SK, Das SK, Deshpande S, Ghude S, Barth M, Rao S, Nanjundiah R, Rajeevan M (2021) Evaluating different lightning parameterization schemes to simulate lightning flash counts over Maharashtra. India Atmos Res 255:105532. ttps://doi.org/10.1016/j.atmosres.2021.105532
51. Morrison H, Thompson G, Tatarskii V (2009) Impact of cloud microphysics on the development of trailing stratiform precipitation in a simulated squall line: Comparison of one- and two-moment schemes. Mon Weather Rev 137:991–1007. ttps://doi.org/10.1175/2008MWR2556.1
52. Mortelmans J, Bechtold M, Brisson E, Lynn B, Kumar S, De Lannoy G (2022) Lightning over Central Canada: skill assessment for various Land-Atmosphere model configurations and lightning indices over a boreal study area. J Geophys Res Atmos 128:e2022JD037236. ttps://doi.org/10.1029/2022jd037236
53. Murugavel P, Pawar SD, Gopalakrishan V (2014) Climatology of lightning over Indian region and its relationship with convective available potential energy. Int J Climatol 34:3179–3187. ttps://doi.org/10.1002/joc.3901
54. National Center for Atmospheric Research (NCAR) (2023) Weather Research and Forecasting (WRF) Model, version 4.5 [Software]. GitHub repository. https://github.com/wrf-model/WRF/tree/release-v4.5
55. Navale A, Singh C (2020) Topographic sensitivity of WRF-simulated rainfall patterns over the North West Himalayan region. Atmos Res 242:105003. ttps://doi.org/10.1016/j.atmosres.2020.105003
56. Niu G, Yang Z, Mitchell KE, Chen F, Ek MB, Barlage M, Kumar A, Manning K, Niyogi D, Rosero E, Tewari M, Xia Y (2011) The community Noah land surface model with multiparameterization options (Noah-MP): 1. Model description and evaluation with local-scale measurements. J Geophys Res Atmos 116:D12109. ttps://doi.org/10.1029/2010jd015139
57. Oulkar S, Siingh D, Saha U, Kamra AK (2019) Distribution of lightning in relation to topography and vegetation cover over the dry and moist regions in the Himalayas. J Earth Syst Sci 128:180. ttps://doi.org/10.1007/s12040-019-1203-9
58. Pawar SD, Gopalakrishnan V, Murugavel P (2015) Role of orography in inducing high lightning flash rate at the foothills of Himalaya. Earth Planets and Space 67:51. ttps://doi.org/10.1186/s40623-015-0221-3
59. Penki RK, Kamra AK (2013) Lightning distribution with respect to the monsoon trough position during the Indian summer monsoon season. J Geophys Res Atmos 118:4780–4787. ttps://doi.org/10.1002/jgrd.50382
60. Petersen WA, Rutledge SA (1998) On the relationship between cloud-to-ground lightning and convective rainfall. J Geophys Res Atmos 103:14025–14040. ttps://doi.org/10.1029/97JD02064

61. Potdar SS, Biswasharma R, Siingh D et al (2026) Coupled Influence of Aerosols, Convection and Cloud Microphysics on Lightning Across Diverse Climatic Regions of India. Int J Climatol e70318. ttps://doi.org/10.1002/joc.70318
62. Potdar SS, Siingh D, Biswasharma R, Gautam AS, Singh R (2025) Influence of land use land cover and topography on lightning distribution over north and north-east Indian region. J Atmos Sol Terr Phys 262:106460. ttps://doi.org/10.1016/j.jastp.2025.106460
63. Price C, Rind D (1992) A simple lightning parameterization for calculating global lightning distributions. J Geophys Res Atmos 97:9919–9933. ttps://doi.org/10.1029/92JD00719
64. Rajeevan M, Kesarkar A, Thampi SB, Rao TN, Radhakrishna B, Rajasekhar M (2010) Sensitivity of WRF cloud microphysics to simulations of a severe thunderstorm event over Southeast India. Ann Geophys 28:603–619. ttps://doi.org/10.5194/angeo-28-603-2010
65. Rosenfeld D, Lensky IM (1998) Satellite-based insights into precipitation formation processes in continental and maritime convective clouds. Bull Am Meteorol Soc 79:2457–2476. ttps://doi.org/10.1175/1520-0477(1998)079
66. Saunders C (2008) Charge separation mechanisms in clouds. Space Sci Rev 137:335–353. ttps://doi.org/10.1007/s11214-008-9345-0
67. Sharma S, Chen Y, Zhou X, Yang K, Li X, Niu X, Hu X, Khadka N (2020) Evaluation of GPMERA satellite precipitation products on the southern slopes of the Central Himalayas against rain gauge data. Remote Sens 12:1836. ttps://doi.org/10.3390/rs12111836
68. Siingh D, Singh AK, Patel RP, Singh R, Singh RP, Veenadhari B, Mukherjee M (2008) Thunderstorms, lightning, sprites and magnetospheric Whistler-Mode radio waves. Surv Geophys 29:499–551. ttps://doi.org/10.1007/s10712-008-9053-z
69. Siingh D, Singh RP, Singh AK, Kulkarni MN, Gautam AS, Singh AK (2011) Solar activity, lightning and climate. Surv Geophys 32:659–703. ttps://doi.org/10.1007/s10712-011-9127-1
70. Siingh D, Singh RP, Singh AK, Kumar S, Kulkarni MN, Singh AK (2012) Discharges in the stratosphere and mesosphere. Space Sci Rev 169:73–121. ttps://doi.org/10.1007/s11214-012-9906-0
71. Siingh D, Singh R, Victor NJ, Kamra A (2023) The DC and AC global electric circuits and climate. Earth-Sci Rev 244:104542. ttps://doi.org/10.1016/j.earscirev.2023.104542
72. Siingh D, Buchunde P, Gandhi H, Singh R, Singh S, Patil M, Singh R (2015) Lightning and convective rain over Indian peninsula and Indo-China peninsula. Adv Space Res 55:1085–1103. ttps://doi.org/10.1016/j.asr.2014.11.014
73. Skamarock WC, Klemp JB (2008) A time-split nonhydrostatic atmospheric model for weather research and forecasting applications. J Comput Phys 227:3465–3485. ttps://doi.org/10.1016/j.jcp.2007.01.037
74. Storelvmo T, Tan I (2015) The Wegener-Bergeron-Findeisen process - Its discovery and vital importance for weather and climate. Meteorol Z 24:455–461. ttps://doi.org/10.1127/metz/2015/0626

75. Takahashi T (1978) Riming electrification as a charge generation mechanism in thunderstorms. J Atmos Sci 35:1536–1548. ttps://doi.org/10.1175/1520-0469(1978)035
76. Taylor KE (2001) Summarizing multiple aspects of model performance in a single diagram. J Geophys Res Atmos 106:7183–7192. ttps://doi.org/10.1029/2000jd900719
77. Tewari VP, Verma RK, Von Gadow K (2017) Climate change effects in the Western Himalayan ecosystems of India: evidence and strategies. For Ecosyst 4:13. ttps://doi.org/10.1186/s40663-017-0100-4
78. Thompson G, Field PR, Rasmussen RM, Hall WD (2008) Explicit forecasts of winter precipitation using an improved bulk microphysics scheme. Part II: Implementation of a new snow parameterization. Mon Weather Rev 136:5095–5115. ttps://doi.org/10.1175/2008mwr2387.1
79. Tsenova B, Mitzeva R (2008) New parameterization of non-inductive charge transfer based on previous laboratory experiments. Atmos Res 91:79–86. ttps://doi.org/10.1016/j.atmosres.2008.07.001
80. Unnikrishnan C, Pawar S, Gopalakrishnan V (2021) Satellite-observed lightning hotspots in India and lightning variability over tropical South India. Adv Space Res 68:1690–1705. ttps://doi.org/10.1016/j.asr.2021.04.009
81. Vani G, Mohan GM, Hazra A, Pawar SD, Pokhrel S, Chaudhari HS, Konwar M, Saha SK, Mallick C, Das SK, Deshpande S, Ghude SD, Domkawale M, Rao SA, Nanjundiah RS, Rajeevan M (2022) Evaluation and Usefulness of Lightning Forecasts Made with Lightning Parameterization Schemes Coupled with the WRF Model. Weather Forecast 37:709–726. ttps://doi.org/10.1175/waf-d-21-0080.1
82. Wang Y, Yang Y, Jin S (2018) Evaluation of lightning forecasting based on one lightning parameterization scheme and two diagnostic methods. Atmos 9:99. ttps://doi.org/10.3390/atmos9030099
83. Williams ER, Geotis SG, Renno N, Rutledge SA, Rasmussen E, Rickenbach T (1992) A radar and electrical study of tropical hot towers. J Atmos Sci 49:1386–1395. ttps://doi.org/10.1175/1520-0469(1992)049<1386:ARAESO>2.0.CO;2
84. Williams E, Stanfill S (2002) The physical origin of the land-ocean contrast in lightning activity. C R Phys 3:1277–1292. ttps://doi.org/10.1016/s1631-0705(02)01407-x
85. Wong J, Barth MC, Noone D (2013) Evaluating a lightning parameterization based on cloud-top height for mesoscale numerical model simulations. Geosci Model Dev 6:429–443. ttps://doi.org/10.5194/gmd-6-429-2013
86. Yadava PK, Sharma A, Payra S, Mall RK, Verma S (2023) Influence of meteorological parameters on lightning flashes over Indian region. J Earth Syst Sci 132:179. ttps://doi.org/10.1007/s12040-023-02188-w
87. Yair Y, Lynn B, Price C, Kotroni V, Lagouvardos K, Morin E, Mugnai A, Del Carmen Llasat M (2010) Predicting the potential for lightning activity in Mediterranean storms based on the Weather Research and Forecasting (WRF) model dynamic and microphysical fields. J Geophys Res Atmos 115:D04205. ttps://doi.org/10.1029/2008jd010868

88. Yang Z, Niu G, Mitchell KE, Chen F, Ek MB, Barlage M, Longuevergne L, Manning K, Niyogi D, Tewari M, Xia Y (2011) The community Noah land surface model with multiparameterization options (Noah-MP): 2. Evaluation over global river basins. J Geophys Res Atmos 116:D12110. ttps://doi.org/10.1029/2010jd015140
89. Zepka G, Pinto O, Saraiva A (2014) Lightning forecasting in southeastern Brazil using the WRF model. Atmos Res 135–136:344–362. ttps://doi.org/10.1016/j.atmosres.2013.01.008
90. Zhao C, Zhang Y, Zheng D, Li H, Du S, Peng X, Liu X, Zha P, Zheng J, Shi J (2024) Technical note: On the ice microphysics of isolated thunderstorms and non-thunderstorms in southern China - a radar polarimetric perspective. Atmos Chem Phys 24:11637–11651. ttps://doi.org/10.5194/acp-24-11637-2024
91. Supplementary Fig and Tables

Figures

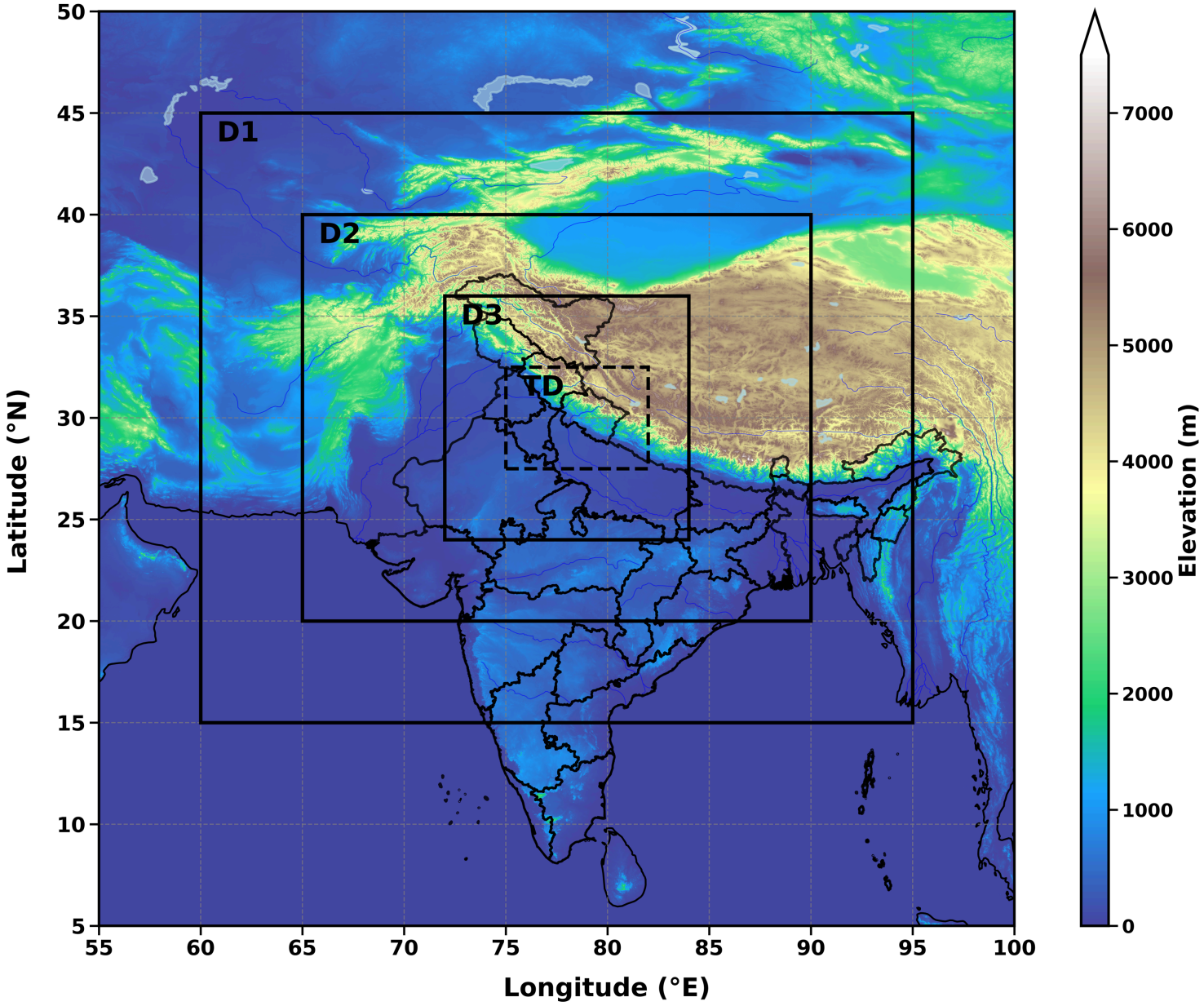


Figure 1

WRF model domain configuration (D1:27 km; D2:9km, D3:3km, Targeted domain: TD) overlaid on a topographic map of India.

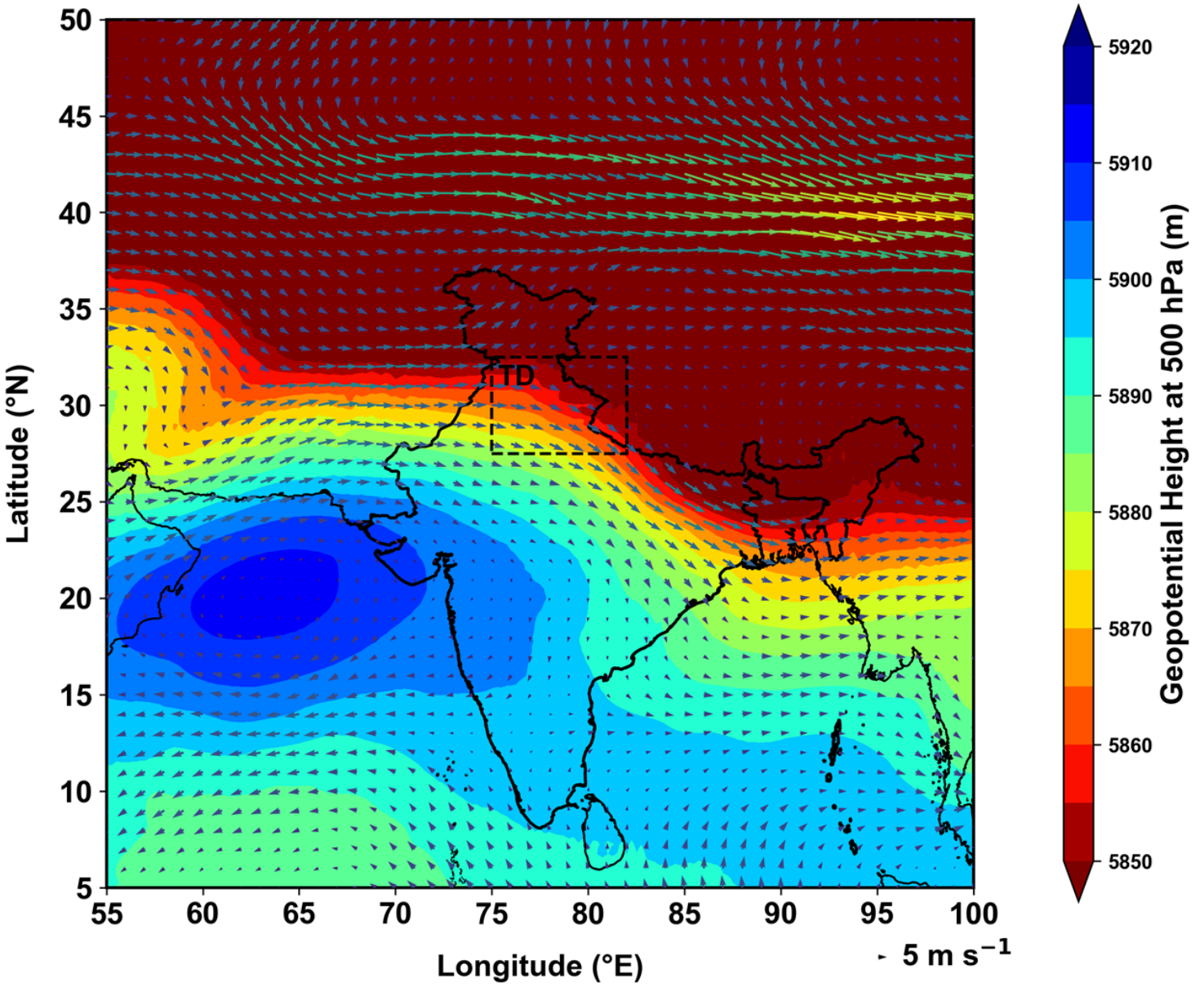


Figure 2

The geopotential height (m) and wind vectors (m s^{-1}) at 500 hPa on 23 May 2023 over India and adjacent areas

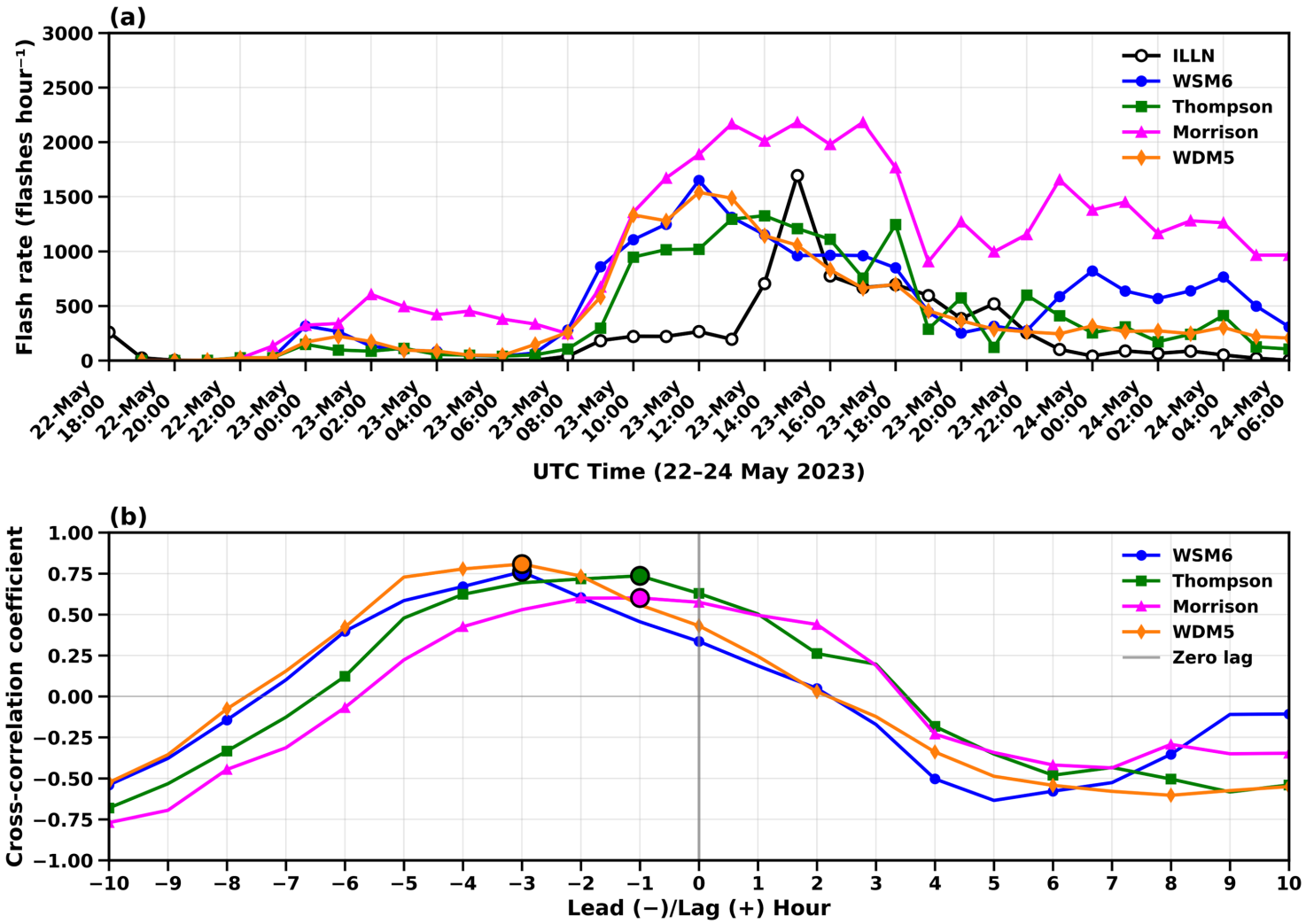


Figure 3

Temporal variation of (a) ILLN observed and model simulated (WSM6, Thompson, Morrison, and WDM 5) flash rate (Flashes hour^{-1}) and (b) cross correlation analysis over the TD domain

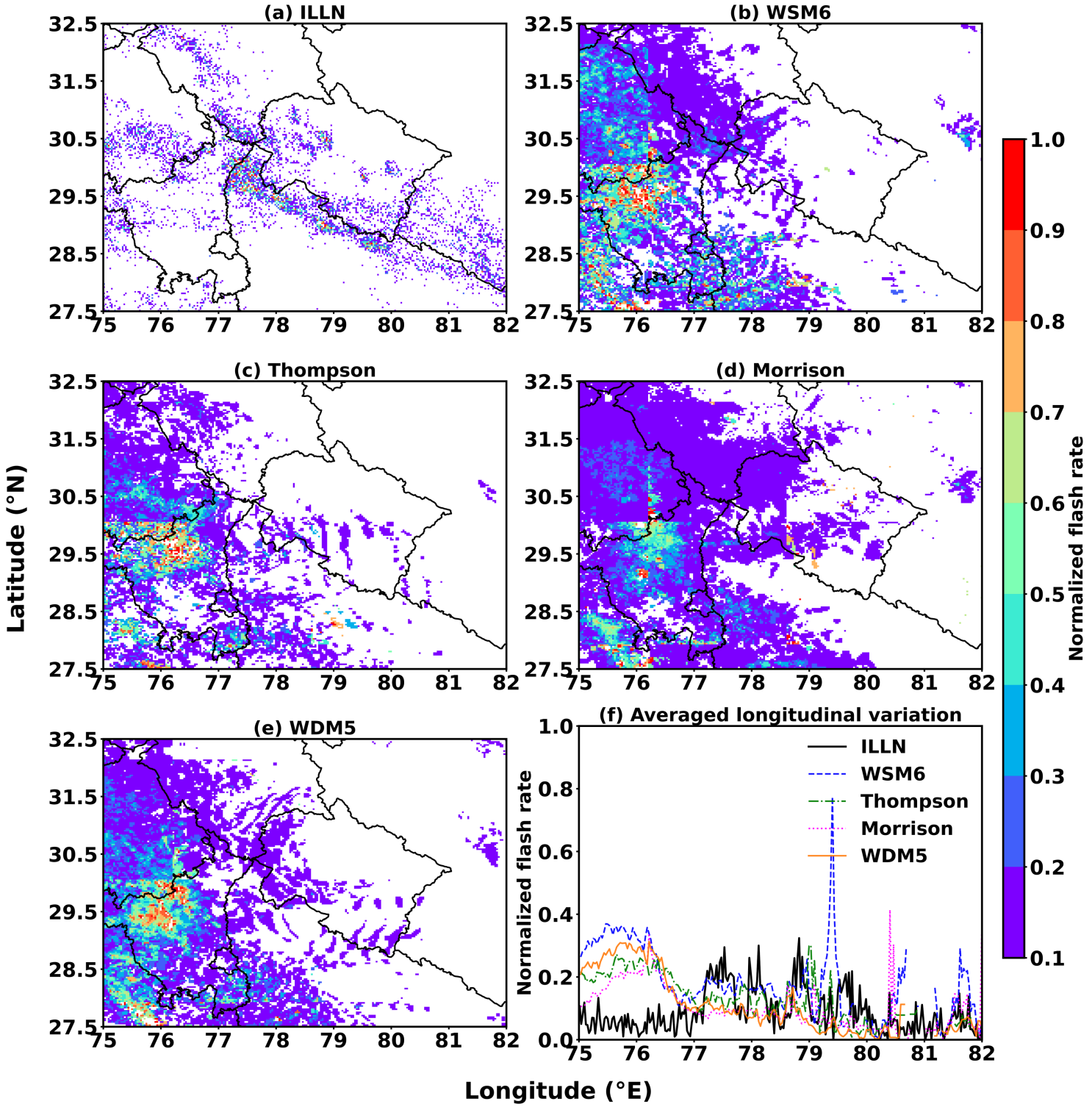


Figure 4

Variation in normalized flash rate from (a) ILLN, (b) WSM6, (c) Thompson, (d) Morrison, (e) WDM5 MP schemes and (f) longitudinal variation over the 3 km grid (TD)

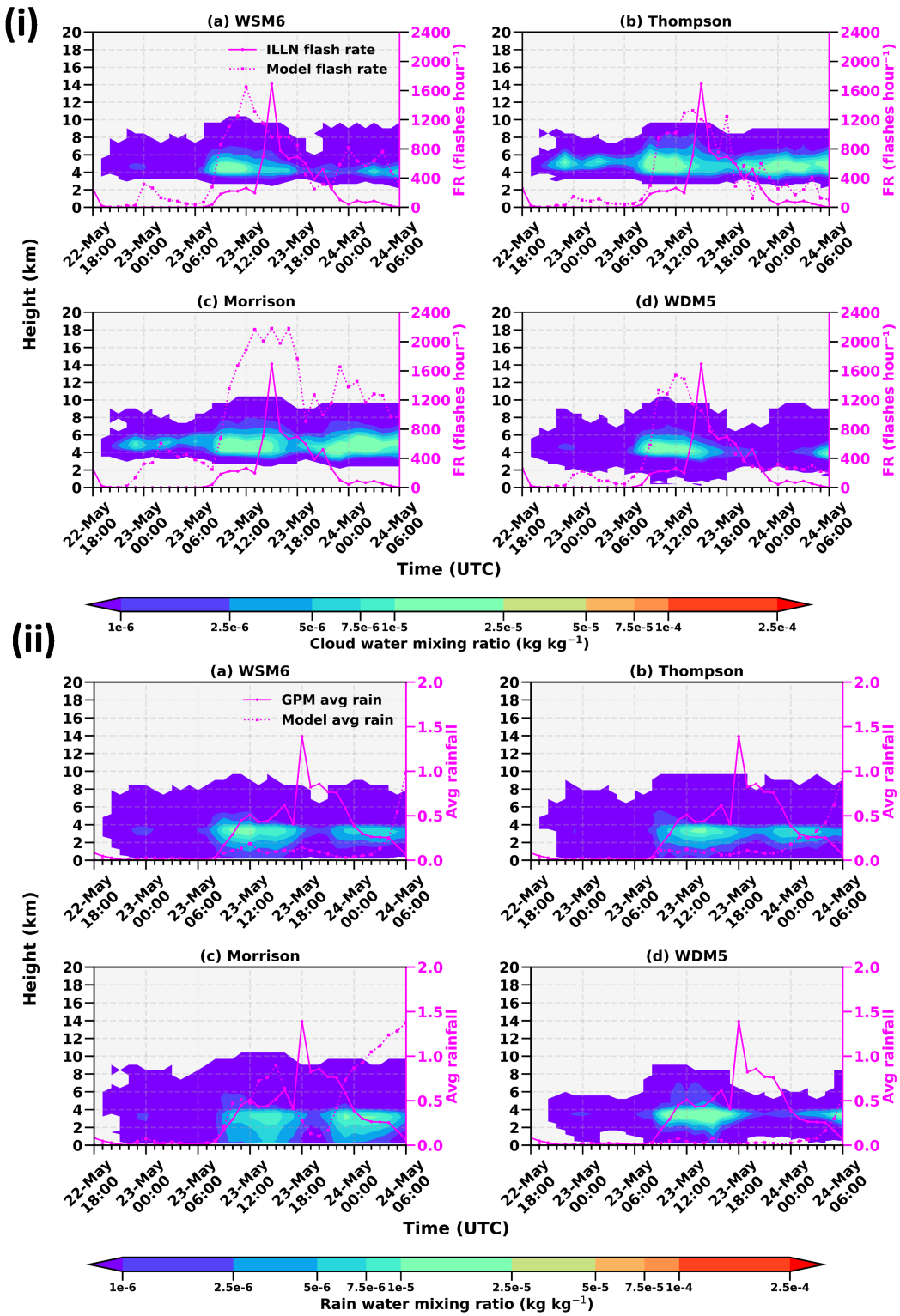


Figure 5

Time-height distributions of (i) Cloud Water Mixing Ratio (q_c) by using (a) WSM6, (b) Thompson, (c) Morrison and (d) WDM5 MP schemes. The solid Magenta line is the observed lightning flash rate by ILLN, and the Magenta dotted line represents the model-generated flash rate in specific MP schemes. Same for (ii) rainwater mixing ratio with GPM rainfall (solid lines) and Model (doted) accumulated rainfall.

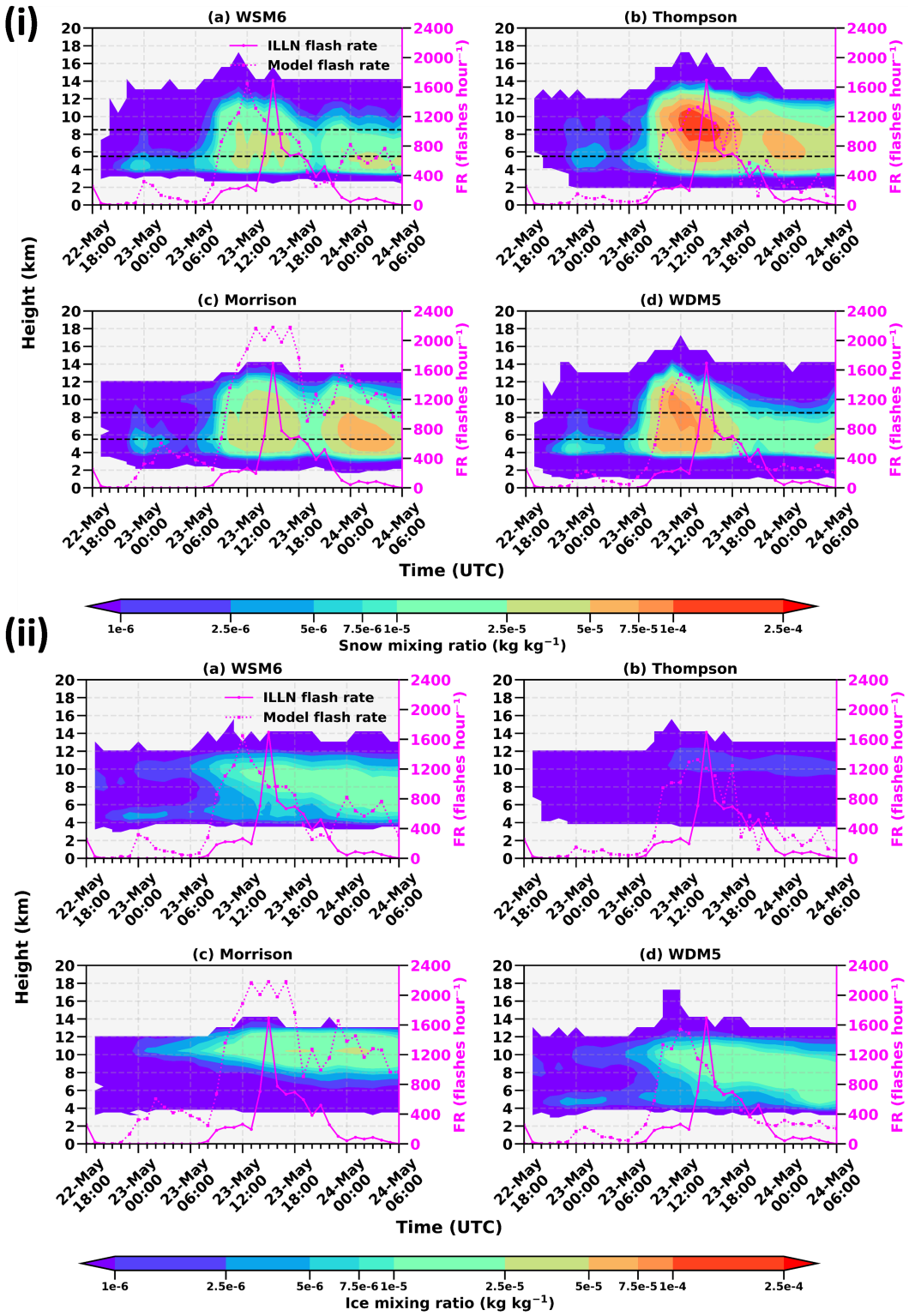


Figure 6

Vertical distribution of (i) snow mixing ratio by using (a) WSM6, (b) Thompson, (c) Morrison and (d) WDM5 MP scheme and the same for (ii) ice mixing ratio. Horizontal dashed lines represent the mixed-phase regions (approximately) in snow mixing ratio

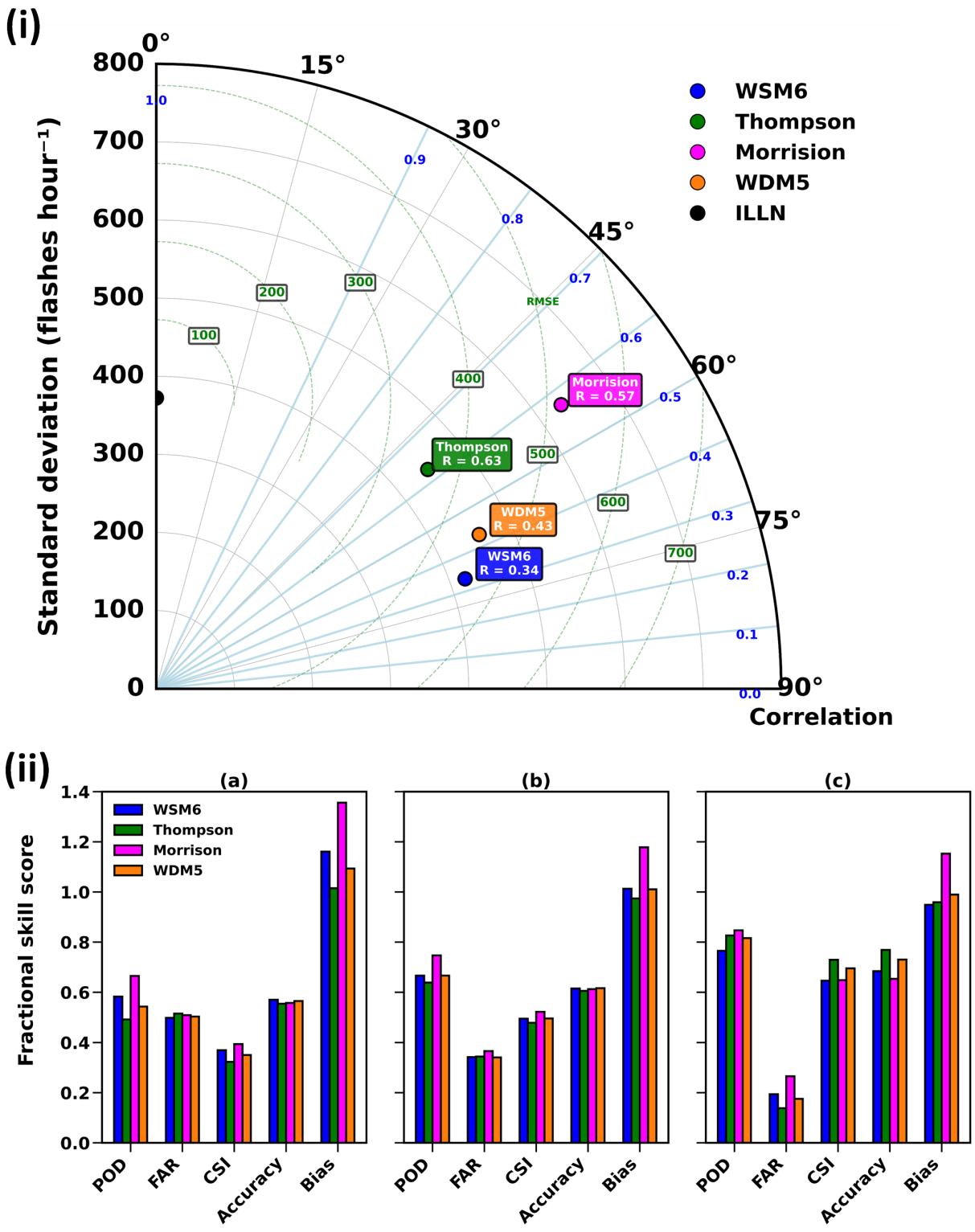


Figure 7

Evaluation of (i) Temporal Model Performance by Taylor diagram analysis. The radial distance in black shows standard deviation and green doted concentric circles show RMSE. The angular position represents the correlation coefficient. (ii) Comparison of different MP schemes and their performance for lightning over TD domain by using (a) 15 km, (b) 21 km, (c) 51 km grid

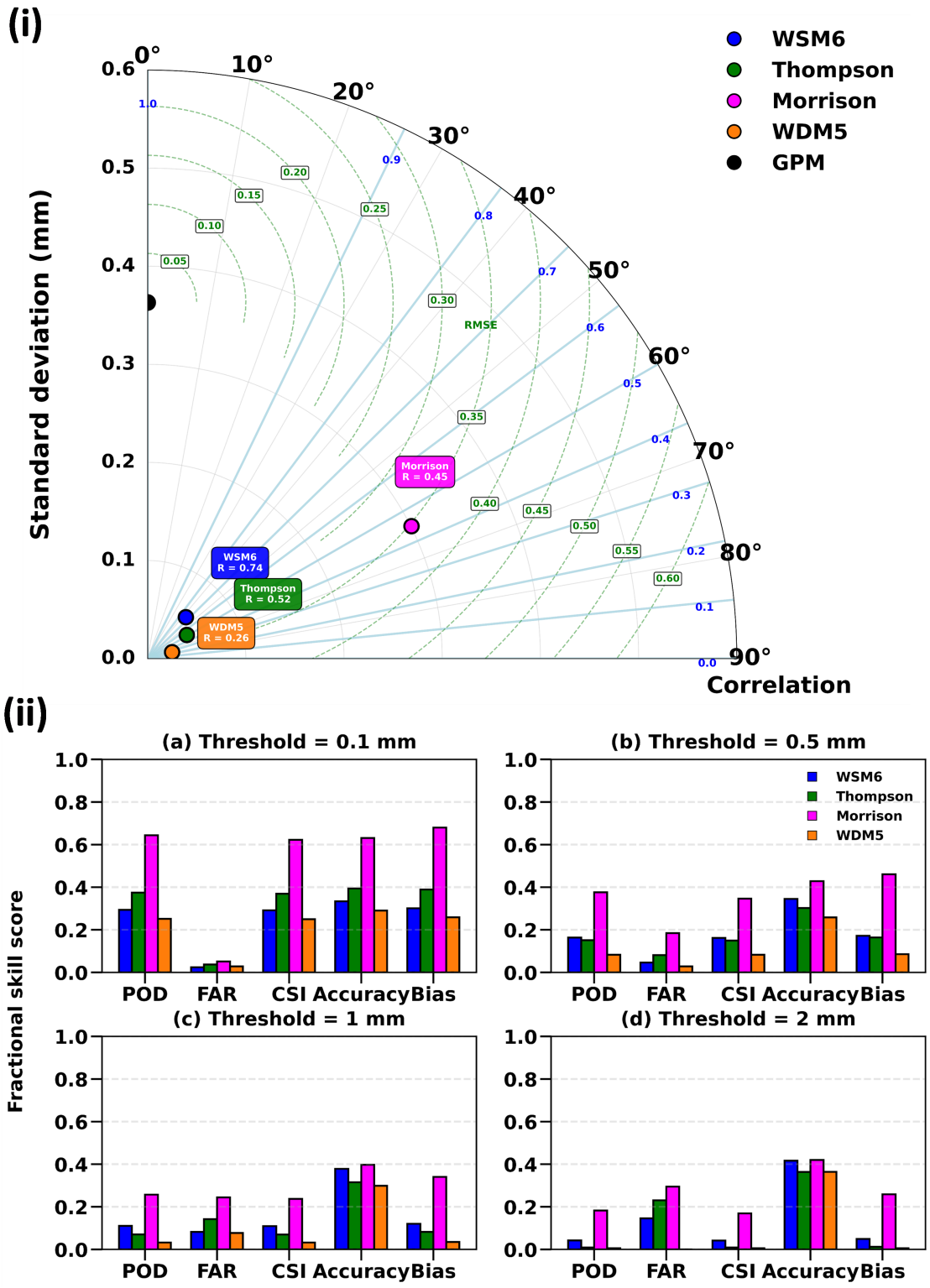


Figure 8

Evaluation of (i) temporal Taylor diagram analysis and (ii) Spatial performance by using fractional skill scores at (a) 0.1 mm, (b) 0.5 mm, (c) 1 mm and (d) 2mm threshold for rainfall prediction

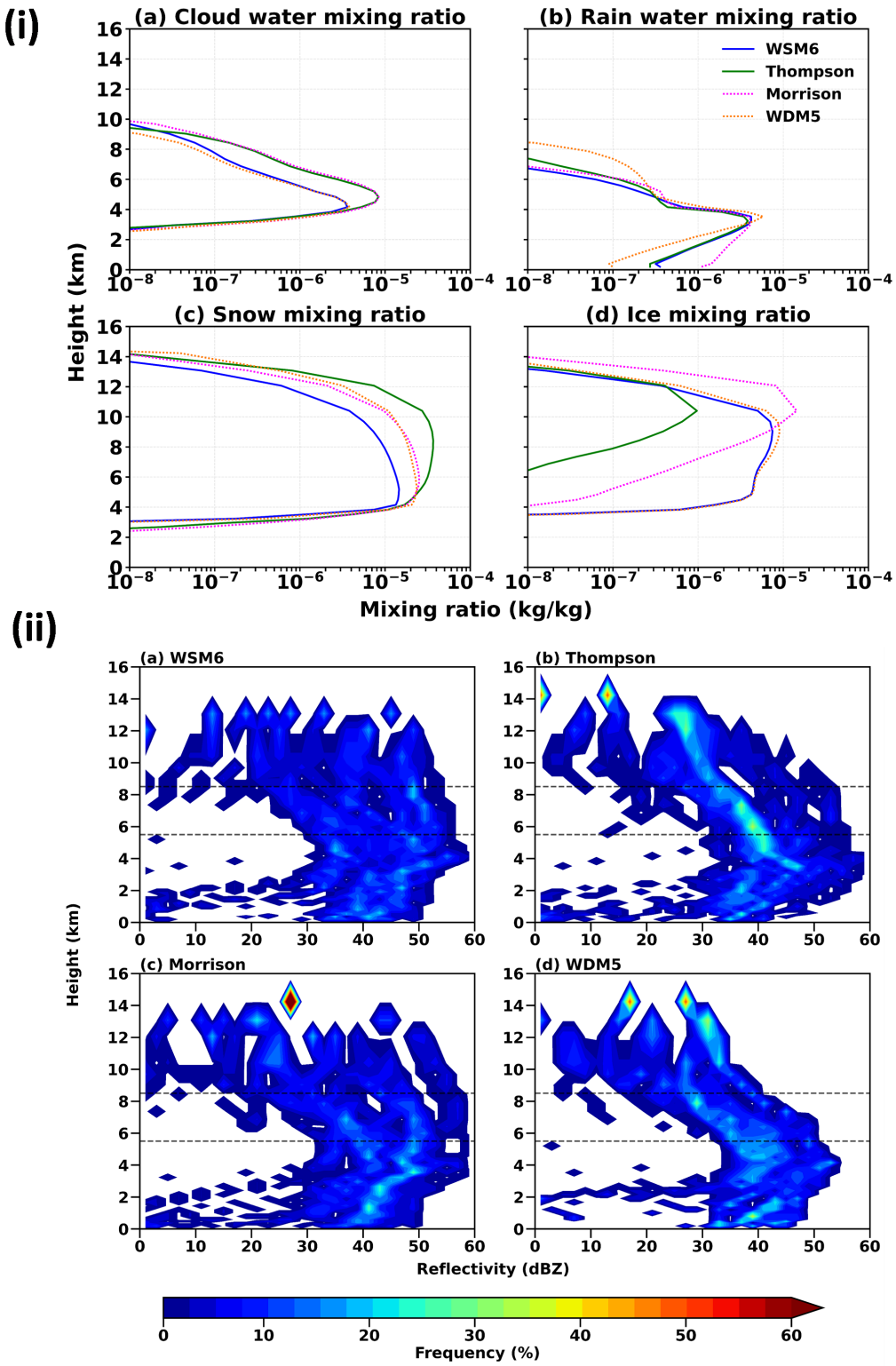


Figure 9

Vertical profiles of domain-averaged (i) mixing ratios of (a) cloud water, (b) rainwater, (c) snow, and (d) ice simulated using the WSM6, Thompson, Morrison, and WDM5 microphysics schemes during the active phase of the thunderstorm. The profiles highlight scheme-dependent differences in the vertical distribution of hydrometeors, with Thompson showing enhanced mixed-phase hydrometeors that favor lightning generation, while WSM6 shows stronger low-level rainwater production associated with more

efficient rainfall processes. (ii) Contoured Frequency by Altitude Diagrams (CFADs) of simulated radar reflectivity for (a) WSM6, (b) Thompson, (c) Morrison, and (d) WDM5 microphysics schemes during the active convective phase. The CFADs illustrate scheme-dependent differences in storm vertical structure, with Thompson exhibiting deeper and more coherent reflectivity cores in the mixed-phase region, favorable for lightning generation, while WSM6 shows stronger low-level reflectivity associated with efficient rainfall production.

Supplementary Files

This is a list of supplementary files associated with this preprint. Click to download.

- SupplementaryFigtables.docx